Hindawi Publishing Corporation
Shock and Vibration
Volume 2016, Article ID 9218317, 11 pages
http://dx.doi.org/10.1155/2016/9218317

Research Article

Performance of Seismic Restrainer with SMA Springs for Sliding Isolation of Single-Layer Spherical Lattice Shells

Peng Zhuang[1,2] and Wenting Wang[1]

[1]*School of Civil and Transportation Engineering, Beijing University of Civil Engineering and Architecture, Zhanlanguan Road 1, Beijing 100044, China*
[2]*Beijing Higher Institution Engineering Research Center of Structural Engineering and New Materials, Beijing University of Civil Engineering and Architecture, Zhanlanguan Road 1, Beijing 100044, China*

Correspondence should be addressed to Peng Zhuang; zhuang_peng@sina.com

Received 18 July 2016; Accepted 15 September 2016

Academic Editor: Mario Terzo

The seismic response of a single-layer spherical lattice shell controlled by restorable sliding isolator is studied under different seismic excitations. The isolation system consists of flat steel-Teflon sliding isolators and superelastic SMA spring restrainers. The NiTi-SMA is used to fabricate helical spring for recentering control of the isolation system. In the first step of this investigation, the configuration scheme and functioning mechanism of a novel SMA spring restrainer are introduced briefly. Then, realistic mechanical behavior of large-scale superelastic NiTi helical spring is studied through a set of cyclic experimental tests. According to the obtained hysteresis loops, a mechanical model combining multilinear model and hysteresis model is developed to simulate the overall response of the SMA-based seismic restrainer. Besides, the sliding isolator is evaluated using a bilinear force-displacement hysteresis model. Finally, a 60 m span single-layer spherical lattice shell with substructure is modeled with finite element program. Nonlinear time history analyses of the controlled and uncontrolled lattice shell are performed considering multidimensional seismic inputs. The study shows that the seismic response of the controlled lattice shell can be effectively reduced by using isolation and control devices. Furthermore, the seismic response of the isolation system such as peak displacement and residual displacement can be effectively controlled by using the developed SMA spring restrainers.

1. Introduction

Seismic isolation theory and technology have developed rapidly and become an effective way to improve seismic performance of buildings and bridges. In addition, the postdisaster cost for repair and rehabilitation of engineering structures can be substantially reduced by using seismic isolation devices. As a result, seismic isolation has been considered as a reliable and cost-effective technology for protecting civil engineering structures from seismic damage. An isolation system primarily is composed of isolators and energy dissipation devices. Nowadays, two types of seismic isolators are widely used [1]: (1) laminated rubber bearings and (2) sliding isolation bearings. Mostly, four types of auxiliary devices are currently employed [2]: (1) viscous devices; (2) elastoplastic devices; (3) viscoelastic devices; and (4) friction devices.

To develop high performance isolation control devices, several researchers have proposed the use of smart materials for structural control. Recently, there has been an increasing interest in utilizing superelastic SMA devices for the development of new seismic isolation systems [3–6]. Although the analytical and experimental studies have proven that the structures with superelastic SMA components usually in the form of wires and bars improve the seismic response [7–10], further research of large-scale SMA element is necessary to fully explore the possibility of applying SMA in seismic control of engineering structures. Regarding the most current SMA-based isolation system, a main drawback is that very long SMA wires and bars have to be adopted. The solutions of configurations of SMA wires or SMA bars in the isolation device proposed in previous work are perhaps applicable only for small displacements. To overcome limitations related to seismic application in realistic building scenarios, some

researchers suggested the use of superelastic SMA helical spring instead of SMA wires or SMA bars as energy dissipation and recentering control system. For example, Speicher et al. [11] developed a tension/compression damper making use of SMA helical springs, which provide stable recentering and damping characteristics. Attanasi and Auricchio [12] proposed conceptual design of an innovative restorable isolation system in which a sliding bearing is coupled with superelastic SMA helical springs that function for recentering purposes.

Most of the previous studies were focused on the development and application of SMA helical springs for isolation and control of multistory buildings. However, very few attempts have been given to the investigation of behavior of long span and spatial structures that are isolated by seismic isolators and controlled by large-scale SMA helical spring devices. The primary objective of this study is to carry out an investigation on feasibility and efficiency of a new type of seismic restrainer with SMA springs that is installed between substructure and spherical lattice shell roof to reduce structural responses. The proposed isolation system for spatial lattice structures consists of a flat sliding isolator and superelastic SMA restrainers. The use of flat sliding bearing can reduce the structural response by limiting the force transfer from the substructure to the superstructure. Beside, such bearings provide dissipation of the seismic energy due to friction mechanism. However, the flat sliding bearings alone do not have any recentering capability and may generate significant residual displacement. A new type of SMA helical spring restrainers is proposed to provide recentering mechanism and additional energy dissipation ability. The conceptual design and the functioning mechanism of the SMA spring restrainer are described. A mechanical model is derived to capture the hysteretic behavior of superelastic SMA helical spring restrainer. In order to investigate mechanical behaviors of the developed device, such seismic restrainers are introduced in spherical lattice shell structures isolated by flat sliding isolators. A set of nonlinear time history analyses using SAP2000 software are performed to examine the effectiveness of the developed SMA-based device in reducing and controlling the response of seismically excited single-layer spherical lattice shell with substructure.

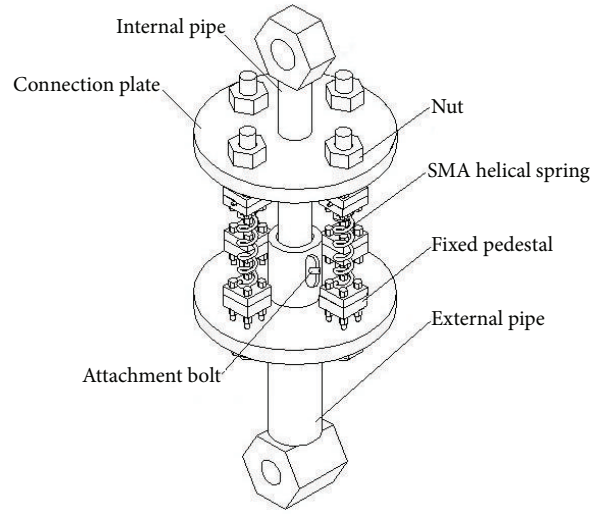

Figure 1: Schematic diagram of SMA spring restrainer.

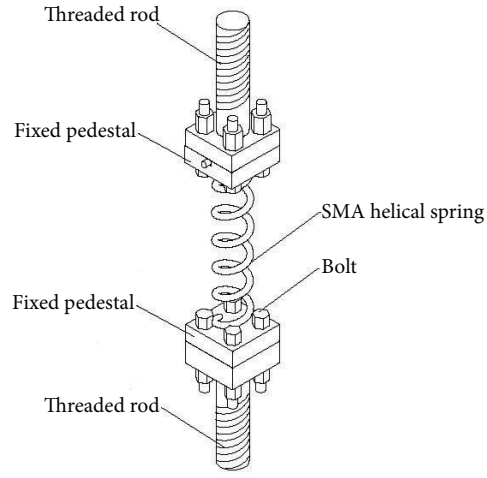

Figure 2: Configuration of the clamping system.

2. Conceptual Design of SMA Spring Restrainer

The SMA spring restrainer device considered in this study primarily consists of several large diameter SMA helical springs. Figure 1 shows a schematic diagram of the developed seismic restrainer. In the design of the seismic restrainer, superelastic SMA helical springs work parallel to provide the recentering property and the additional energy dissipation capability. Such SMA helical springs are fixed to the connection plate through clamping system and nuts. A particular clamping system is used to connect ends of the SMA springs to the other elements, as shown in Figure 2. The ends of the SMA helical springs are fastened by using the fixed pedestals and the threaded rods. According to the design, the hook-like ends of the spring are mounted in the inner slots of the fixed pedestals, and the superelastic springs are clamped by tightening the screws on the fixed pedestal. Then, the threaded rods are fastened to the connection plate of the damper. It is observed that the installation and replacement of the SMA spring elements are convenient to be implemented. Besides, the attachment bolt in the control device is employed to prevent too large axial deformation of the device.

When both ends of the seismic restrainer move mutually, the SMA springs are stretched and shortened. The manners above provide the new control device with necessary energy dissipation ability and recentering capacity. The proposed control device can be used as link element in spatial lattice structures. In engineering application, the design parameters of the SMA spring restrainer, such as the number, the configuration, and the dimensions of the SMA helical spring, can be determined in accordance with the practical requirements.

Figure 3: Large-scale SMA helical spring.

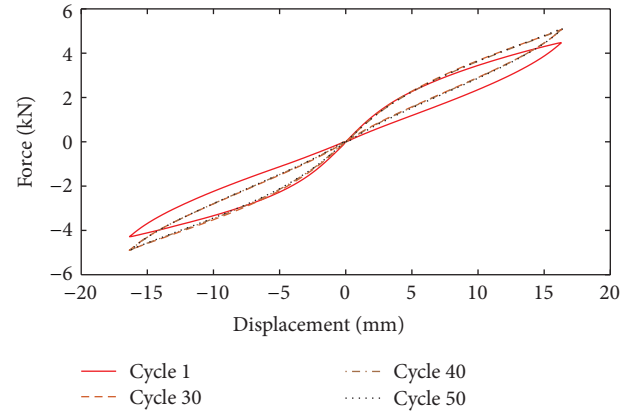

Figure 4: Hysteresis loops at different loading cycles.

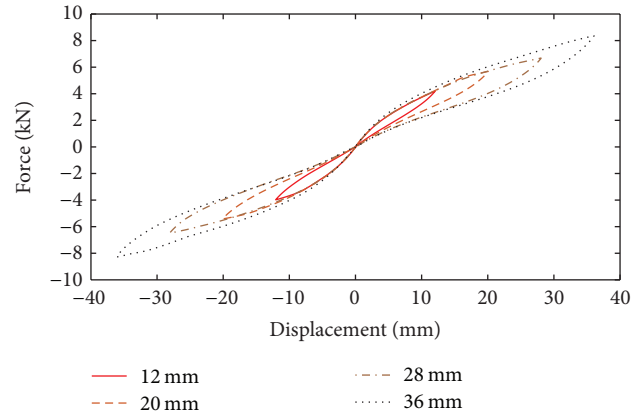

Figure 5: Hysteresis loops at different displacement amplitudes.

3. Modeling of the Seismic Restrainer

3.1. Superelastic Behavior of SMA Helical Spring. A type of large-scale superelastic SMA helical spring is fabricated and a set of cyclic experimental tests for the developed SMA element are executed to understand its realistic nonlinear behavior. The NiTi-SMA ($Ni_{50.8}Ti_{49.8}$, atom ratio) is used in this experimental study. The martensite start temperature M_s, the martensite finish temperature M_f, the austenite start temperature A_s, and the austenite finish temperature A_f of the SMA are $M_s = -61.3^{\circ}C$, $M_f = -40.0^{\circ}C$, $A_s = -29.9^{\circ}C$, and $A_f = -12.6^{\circ}C$. The large-scale tension/compression SMA helical spring is made from the above-described NiTi alloy. The SMA helical spring with a free length of 350 mm, external diameter of 36 mm, and wire diameter of 12 mm was tested in a SANS testing machine, as shown in Figure 3. During the cyclic tension-compression tests, the applied forces and displacements were measured by the inherent sensor of the testing machine.

The mechanical tests were performed at room temperature of about 20°C. First, the test on the SMA specimen was conducted for 50 cycles with 16 mm displacement and 0.1 Hz loading frequency to stabilize the hysteretic loops. Then, the cyclic loading with the amplitudes of cyclic displacement of 12, 20, 28, and 36 mm and 0.2 Hz loading frequency was applied to the spring specimen. The shape of cyclic displacement during the tests was triangle type of waves. Figure 4 presents the force-displacement curves of the SMA helical spring specimens under different cycles. It can be observed that the hysteresis loops of the SMA spring specimen slightly shift with the increased loading cycle number. The hysteresis loops tend to overlap and the superelastic behavior begins to stabilize during the cyclic test case. The experimental force-displacement curves of a single SMA helical spring with hook-like ends at different displacement amplitudes are shown in Figure 5. It can be seen that the superelastic SMA spring shows stable hysteretic behavior without any residual deformation. After tests, the specimen was checked and measured, and the spring was undamaged and the initial geometry was perfectly recovered.

3.2. Mechanical Model of SMA Spring Restrainer. The behaviors of the SMA helical spring can be modeled using solid finite elements incorporating the stress-strain constitutive relationship of SMA material [12, 13]. But it is generally impractical for nonlinear time history analysis of a complete engineering structure through such refined simulation method. This paper develops an alternative modeling technique of the SMA helical spring with a continuous hysteretic system that is more physical and more efficient in describing nonlinear behavior of the SMA spring than the refined models described above.

In this study, the SMA spring is modeled with a combination of two nonlinear elements to simulate the superelastic behavior. The model consists of the following components.

Element I: Nonlinear Elastic Element. This element is used to capture the stiffness property of the SMA spring under cyclic loading-unloading process. As shown in Figure 6(a),

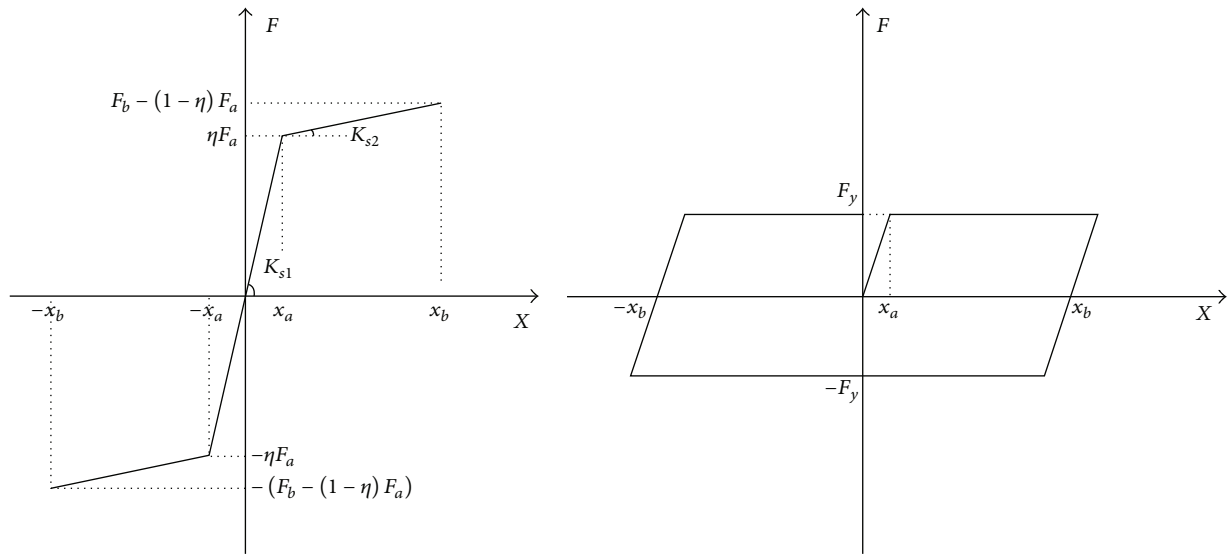

(a) Nonlinear elastic element (b) Hysteretic model

Figure 6: Schematic diagram of theoretical model of SMA spring.

the computational model of the nonlinear elastic element is given by

$$F_{\mathrm{ml}} = \begin{cases} \pm K_{s1}|x| & |x| \le x_a \\ \pm\left[K_{s1}x_a + K_{s2}\left(|x| - x_a\right)\right] & x_a < |x| \le x_b, \end{cases} \tag{1}$$

where F_{ml} is the restoring force provided by the nonlinear elastic element; x is the displacement of the nonlinear elastic element; x_a is the yield displacement; x_b is the design displacement; K_{s1} is the initial stiffness of the nonlinear elastic element computed from the following equation:

$$K_{s1} = \frac{(\eta F_a)}{x_a}, \tag{2}$$

Where η is the ratio between $F_{\mathrm{ml}}(x_a)$ and F_a and can be obtained by trial and adjustment; K_{s2} is the postyielding stiffness of the nonlinear elastic element calculated by

$$K_{s2} = \frac{\left[F_b - (1-\eta)F_a\right]}{(x_b - x_a)}. \tag{3}$$

Element II: Hysteretic Element. This element describes an elastoplastic behavior with a smooth transition from the elastic to plastic range, which is used to account for the energy dissipation capacity of the SMA spring. The element, as shown in Figure 6(b), is based on the Bouc-Wen model [14], and its force-displacement relation can be given as follows:

$$F_w = \alpha\frac{F_y}{x_a}x + (1-\alpha)F_y z, \tag{4}$$

where F_w is the restoring force provided by the hysteretic element; $F_y = (1-\eta)F_a$ is the yield force of the hysteretic element; α is the ratio of the postyielding to elastic stiffness; z is the hysteretic dimensionless quantity expressed as

$$x_a\dot{z} + \gamma|\dot{x}|z|z|^{n-1} + \beta\dot{x}|z|^n - A\dot{x} = 0, \tag{5}$$

where γ, β, A, and n are dimensionless parameters that control the shape of the hysteresis loop.

The nonlinear elastic element and the hysteretic element work in parallel under the same displacement to provide an overall restoring force of the SMA helical spring, which can be computed as

$$F_{\mathrm{SMA}} = F_{\mathrm{ml}} + F_w, \tag{6}$$

where F_{SMA} is the restoring force of the superelastic SMA spring.

The overall restoring force of the superelastic seismic restrainer is the sum of the nonlinear forces provided by the SMA helical springs, which is given by

$$F_{\mathrm{SR}} = \sum_{j=1}^{n} F_{sj}, \tag{7}$$

where F_{SR} denotes the restoring force of the seismic restrainer; F_{sj} represents the restoring force of the jth SMA helical spring.

In this study, the parameters of the theoretical model of the SMA spring specimens have been selected by fitting experimental hysteresis loops from the aforementioned cyclic tests obtained at various displacement amplitudes ranging from 12 to 36 mm. A MATLAB-based program was developed and employed to describe response of the tested SMA specimens. Figure 7 demonstrates the hysteretic loops together with the tests results at the displacement amplitudes of 12, 20, 28, and 36 mm. It is found that the nonlinear hysteretic behavior of the SMA spring can be effectively

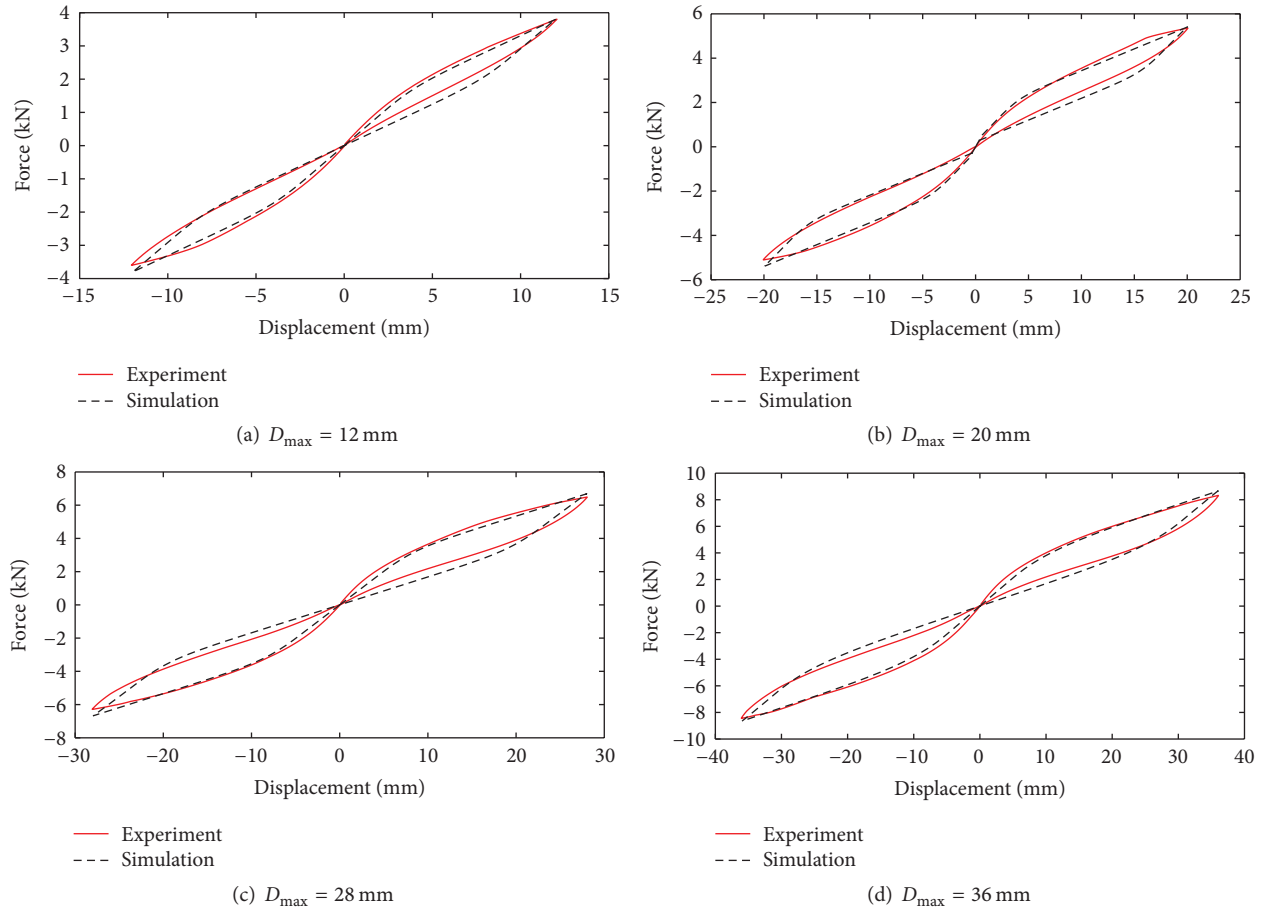

Figure 7: Experimental and numerical hysteretic curves of SMA spring.

simulated. As shown in the figure, the simulated curves of both SMA spring specimens agree well with the experimental results.

4. Seismic Analysis of a Controlled Single-Layer Lattice Shell Structure

4.1. Structural Model. To investigate seismic performance of the superelastic restrainer in spatial lattice shell structures, a Kiewitt type of single-layer spherical lattice shell (K8-type) with 8 rings is selected. The spherical lattice shell has a span of 60 m and a height of 10 m. The thickness between upper and lower chords is taken as 2 m. Several types of steel tubes, $\phi 140 \times 8$ and $\phi 180 \times 8$, are selected as the internal steel tube members of the lattice shell structure, which are modeled as beam elements. Besides, $\phi 377 \times 10$ beams are used as the bottom ring members of the spherical lattice shell roof. Under the lattice shell roof, the steel frame including 500 mm×300 mm×20 mm steel box beams and $\phi 480 \times 12$ steel columns are available for supporting the superstructure. All components of the isolator are made of Q345 steel apart from the frictional material and SMA. The hinged supports for the uncontrolled shell and the SMA restrainers for the controlled shell are employed as link component between the lattice shell roof and the substructure.

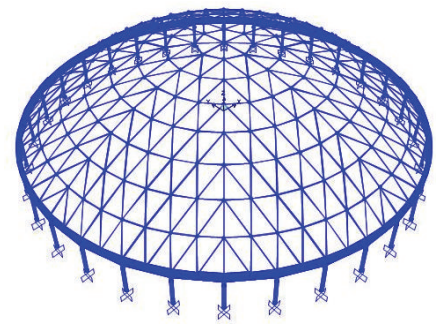

Figure 8: Finite element model of single-layer lattice shell.

In this study, SAP2000 software is applied to establish the structural model and calculate its dynamic response. The finite element model of the lattice shell structure is shown in Figure 8. The roof load is taken as 1.0 kN/m^2. All the loads and self-weight of the structure are treated as lumped masses concentrated at the nodes of the structure. Nonlinear elements such as the nonlinear elastic element and Wen plastic element are combined to simulate the SMA spring in the SAP2000 software, in which the performance parameters of the tested SMA spring specimen are utilized to establish the

Table 1: Values of parameters for nonlinear element of SMA spring restrainer.

Component	Nonlinear element	Performance parameters			
		Yield force (kN)	Yield displacement (mm)	Post yield stiffness ratio	Yield exponent
SMA springs	Multi-linear elastic	7.45	2	0.594	—
	Plastic (Wen)	5	2	0	2

numerical model. The sliding isolator is simulated by friction isolator element in SAP2000.

4.2. Seismic Response Analysis. The performance parameters of the tested SMA helical spring specimen are utilized to establish the damper model. The SMA system in each hybrid device consists of four NiTi-SMA helical springs. The design displacement of the SMA spring restrainer is taken as ±50 mm. Values of the parameters of the nonlinear elements for simulating the SMA restrainer in SAP2000 are listed in Table 1.

The friction isolator element is used to simulate seismic isolation device applied to the single-layer lattice shell structure. The frictional force model for the aforementioned friction isolator is given by [15]

$$F_{fx} = \mu P z_{fx}, \tag{8}$$

$$F_{fy} = \mu P z_{fy}, \tag{9}$$

where μ is the coefficient of friction; P is the normal load carried by the bearing interface; z_{fx} and z_{fy} are hysteretic dimensionless quantities computed from the following differential equations:

$$Y\dot{z}_{fx} = \Omega\dot{u}_b + \theta\left|\dot{u}_b\right| z_{fx}\left|z_{fx}\right|^{q-1} - \lambda\dot{u}_b\left|z_{fx}\right|^{q} = 0, \tag{10}$$

$$Y\dot{z}_{fy} = \Omega\dot{u}_b + \theta\left|\dot{u}_b\right| z_{fy}\left|z_{fy}\right|^{q-1} - \lambda\dot{u}_b\left|z_{fy}\right|^{q} = 0, \tag{11}$$

where Y is the yield displacement; $\dot{u}_b$ is the slip velocity of the isolator; θ, λ, Ω, and q are dimensionless parameters that control the shape of the hysteretic curve. The recommended values of these parameters to provide typical Coulomb friction force are $Y = 0.5$ mm, $\theta = 0.5$, $\lambda = 0.5$, $\Omega = 1$, and $q = 2$. The Coulomb friction coefficient for the friction isolator in structural analysis is taken as 0.10.

Three ground motion records, including the three components (i.e., the NS, EW, and UD components) of El-Centro wave, Taft wave, and Sylmar wave, were selected as seismic inputs in the X, Y, and Z directions, respectively. The peak ground acceleration was scaled to 0.20 g, 0.30 g, and 0.40 g in the simulation, respectively. The ratio of the accelerations in three directions $a_x : a_y : a_z$ =1 : 0.85 : 0.65. Seismic response analyses are performed for the single-layer spherical lattice shell under the conditions with and without seismic control devices corresponding to the controlled shell and the uncontrolled shell, from which seismic responses of both structures and the isolation system have been obtained. To display the controlling effects, reduction ratio for earthquake responses

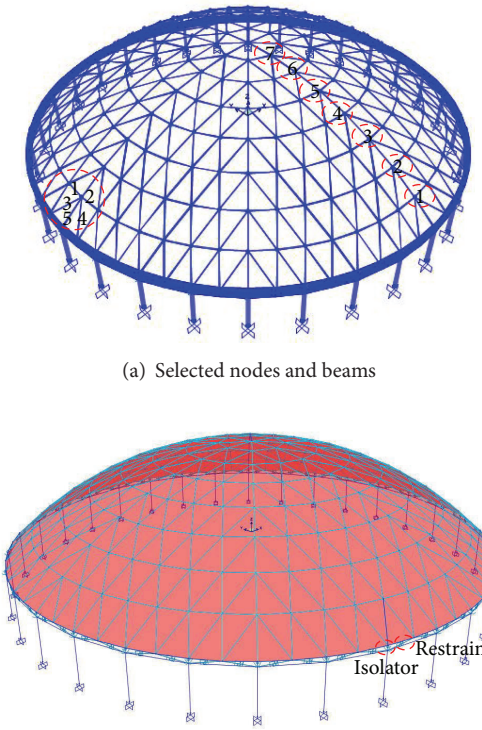

(a) Selected nodes and beams

(b) Selected isolator and restrainer

Figure 9: Selected nodes and elements in the lattice shell.

under different seismic resistance conditions is defined by

$$\text{Reduction ratio } \beta = \frac{(R_1 - R_2)}{R_1}, \tag{12}$$

where R_1 represents the response of the uncontrolled structure; R_2 represents the response of the controlled structure.

The selected nodes and elements for analyzing seismic response characteristics of the lattice shell structure are shown in Figure 9. The responses of the selected nodes along with the height of the roof are used to investigate the seismic control effects for nodal acceleration of the single-layer lattice shell. The selected beams are close to the boundary of the lattice shell and the responses of such element are employed to study the seismic control effect for internal force. Furthermore, an isolator element and a SMA spring restrainer are selected to investigate their seismic response. Figure 10 illustrate the peak value of acceleration in X direction under Sylmar wave for controlled and uncontrolled shell. It is observed that the peak values of acceleration response of the selected nodes are effectively reduced by using the isolation

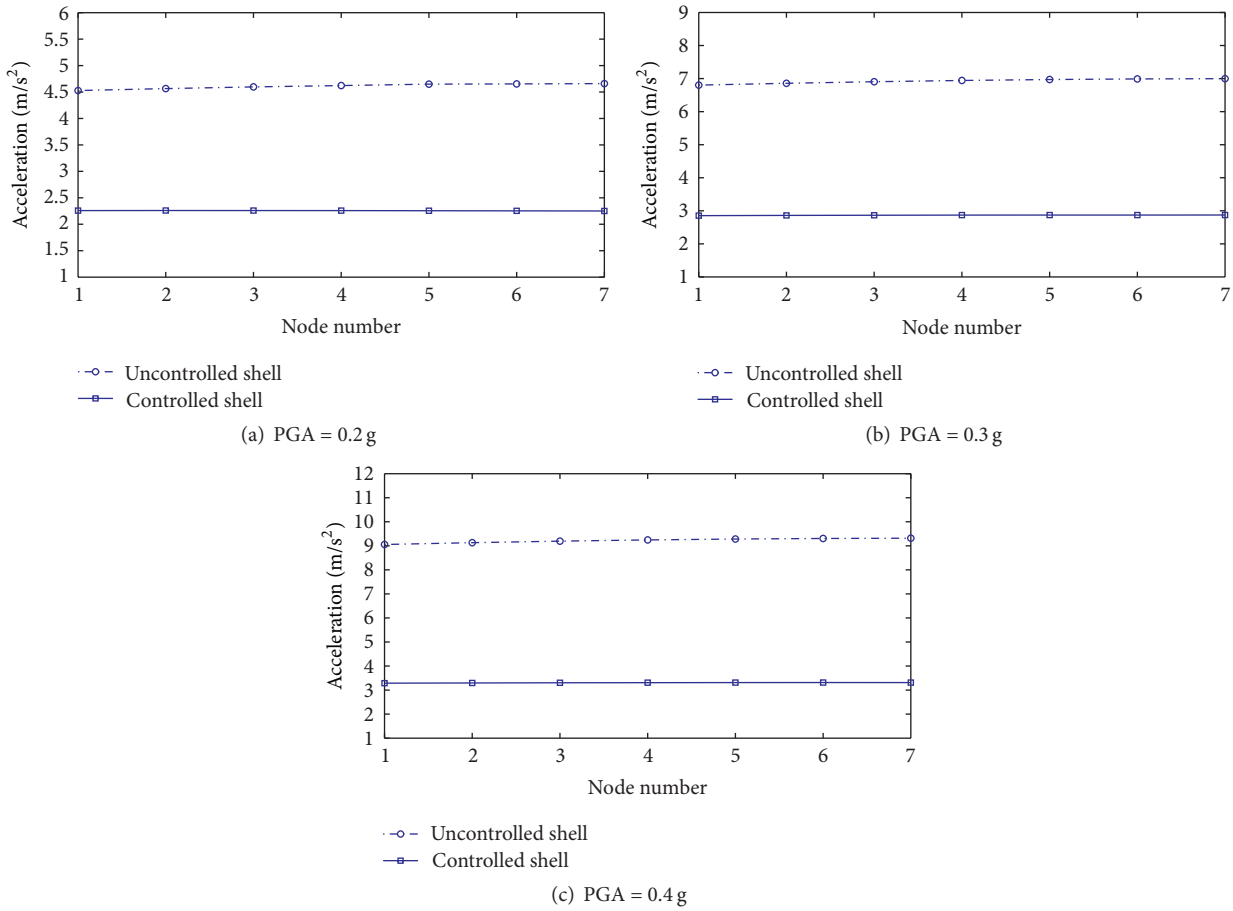

Figure 10: Peak value of acceleration in X direction for selected nodes under Sylmar wave.

Table 2: Control effect of peak base shear in X direction (Units in kN).

Earthquake wave	PGA = 0.2 g			PGA = 0.3 g			PGA = 0.4 g		
	Controlled	Uncontrolled	β	Controlled	Uncontrolled	β	Controlled	Uncontrolled	β
El-Centro	968	1177	0.178	1445	1766	0.182	1906	2353	0.190
Taft	1259	1522	0.173	1478	2120	0.303	1567	2831	0.446
Sylmar	1297	2103	0.383	1530	3158	0.516	1658	4205	0.606

and control devices, and the maximum is decreased from about 9 to 3 m/s^2. The slight variation of acceleration response for the controlled shell with the increasing PGA can also be observed. The range of the nodal acceleration of the uncontrolled shell during this numerical case was from 4.5 to 9 m/s^2. When the hinged supports are replaced by the isolation and control devices, all peak values of acceleration of the selected nodes are reduced to 3.5 m/s^2 and below. Figure 11 shows reduction ratios for acceleration response of the selected nodes in the controlled and uncontrolled lattice shell under various seismic excitations. Note that the isolation and control effect is gradually improved with the increasing seismic input intensities. Tables 2 and 3 give comparisons for peak values and reduction ratios of base shear response of the lattice shell in X and Y directions under different seismic excitations and intensities. The reduction ratio for base shear is gradually enhanced while increasing the ground motion intensities, which is similar to the variation trend for acceleration response. As for other seismic responses of the lattice shell, the peak axial force of beam elements can be effectively reduced by using the isolation and control technology. Tables 4–6 show comparisons for peak values and reduction ratios of axial force of the selected beam elements for the controlled and uncontrolled shell under different earthquake waves. It can be seen that the control effect for axial force of the beam element in the lattice shell roof is still gradually improved with an increase of PGAs. The progressively increased reduction ratio for the abovementioned response quantities is due to the transition from a relatively high initial stiffness to a postyield stiffness of the seismic restrainer and full energy dissipation provided by the isolation and control device when the combined isolation

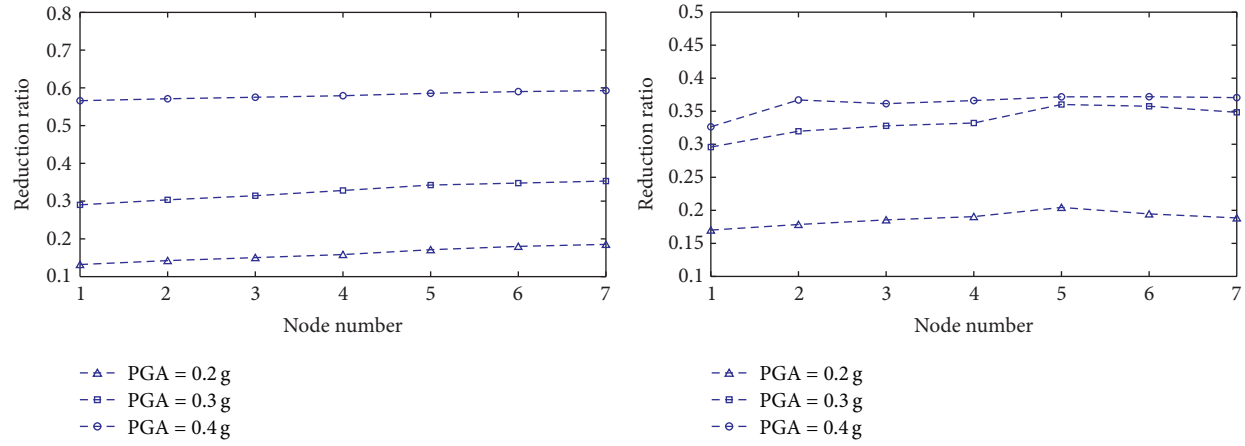

(a) Reduction ratio in X direction under El-Centro wave

(b) Reduction ratio in Y direction under El-Centro wave

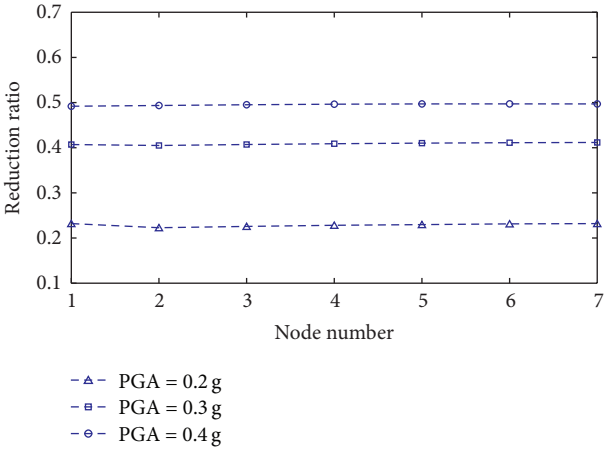

(c) Reduction ratio in X direction under Taft wave

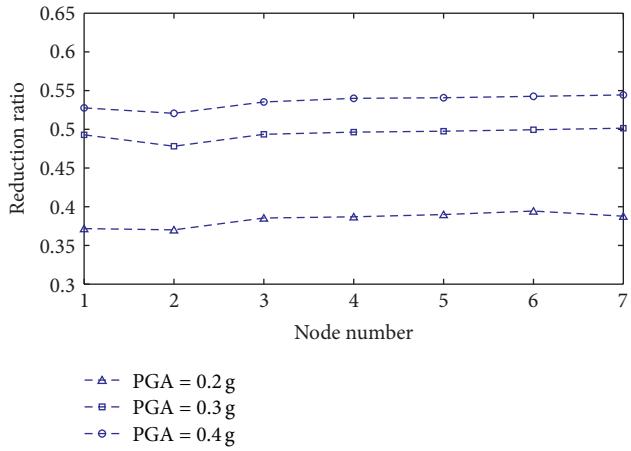

(d) Reduction ratio in Y direction under Taft wave

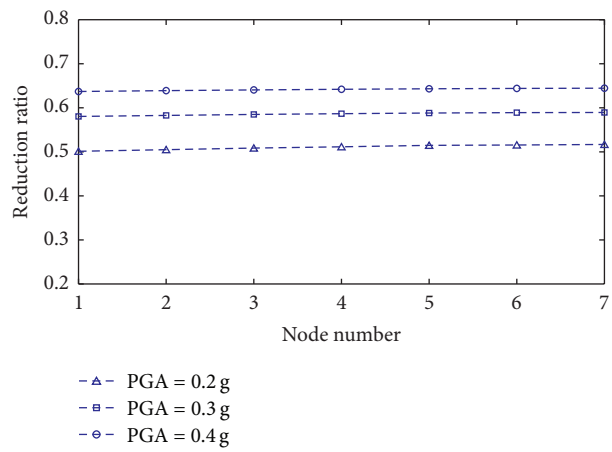

(e) Reduction ratio in X direction under Sylmar wave

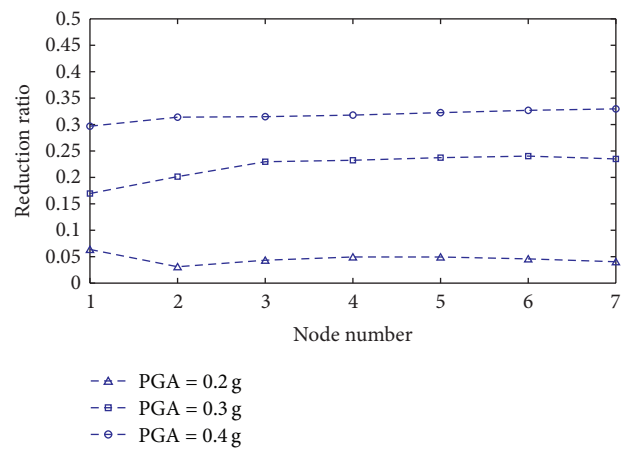

(f) Reduction ratio in Y direction under Sylmar wave

Figure 11: Reduction ratio for peak value of nodal acceleration under various earthquake waves.

system generates large deformation under strong ground motions.

Time histories of the displacement of the flat friction isolator coupled with the SMA spring restrainers of the controlled shell structure subjected to various earthquake waves are shown in Figure 12. Most displacement amplitudes in X direction and in Y direction of the steel-Teflon sliding isolator range from 30 to 50 mm under the 3 ground motion records. As shown in Figure 12, the residual displacements of the isolator are very small and they can be neglected. Figure 13 illustrates the force-displacement hysteresis loops of the installed superelastic NiTi-SMA restrainer under various

Table 3: Control effect of peak base shear in Y direction (units in kN).

Earthquake wave	PGA = 0.2 g			PGA = 0.3 g			PGA = 0.4 g		
	Controlled	Uncontrolled	β	Controlled	Uncontrolled	β	Controlled	Uncontrolled	β
El-Centro	1042	1262	0.174	1502	1879	0.201	2009	2524	0.204
Taft	1090	1565	0.304	1410	2053	0.313	1567	2718	0.423
Sylmar	824	938	0.122	1196	1409	0.151	1672	2076	0.195

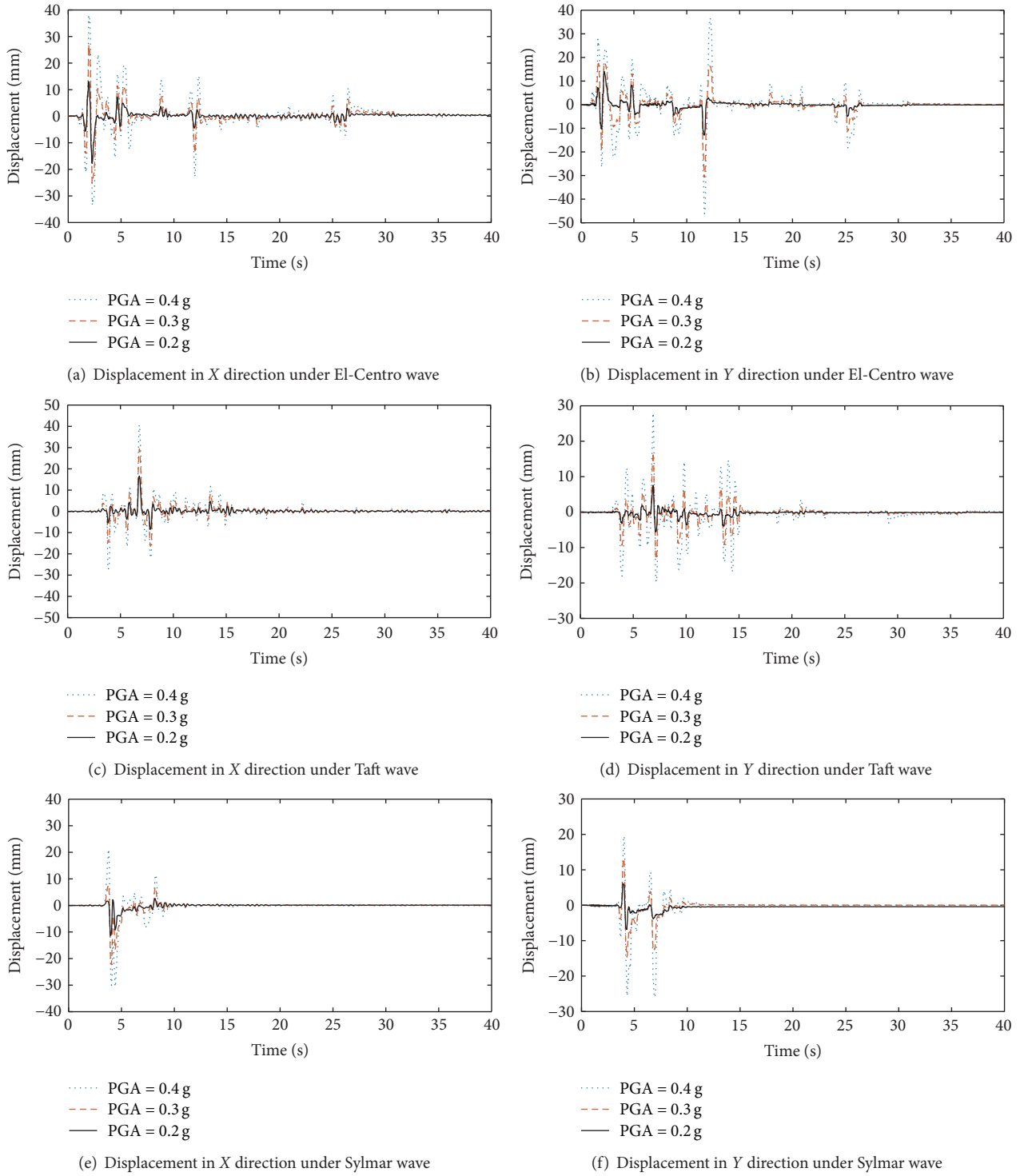

(a) Displacement in X direction under El-Centro wave

(b) Displacement in Y direction under El-Centro wave

(c) Displacement in X direction under Taft wave

(d) Displacement in Y direction under Taft wave

(e) Displacement in X direction under Sylmar wave

(f) Displacement in Y direction under Sylmar wave

Figure 12: Time histories of isolation system displacement subjected to various seismic excitations.

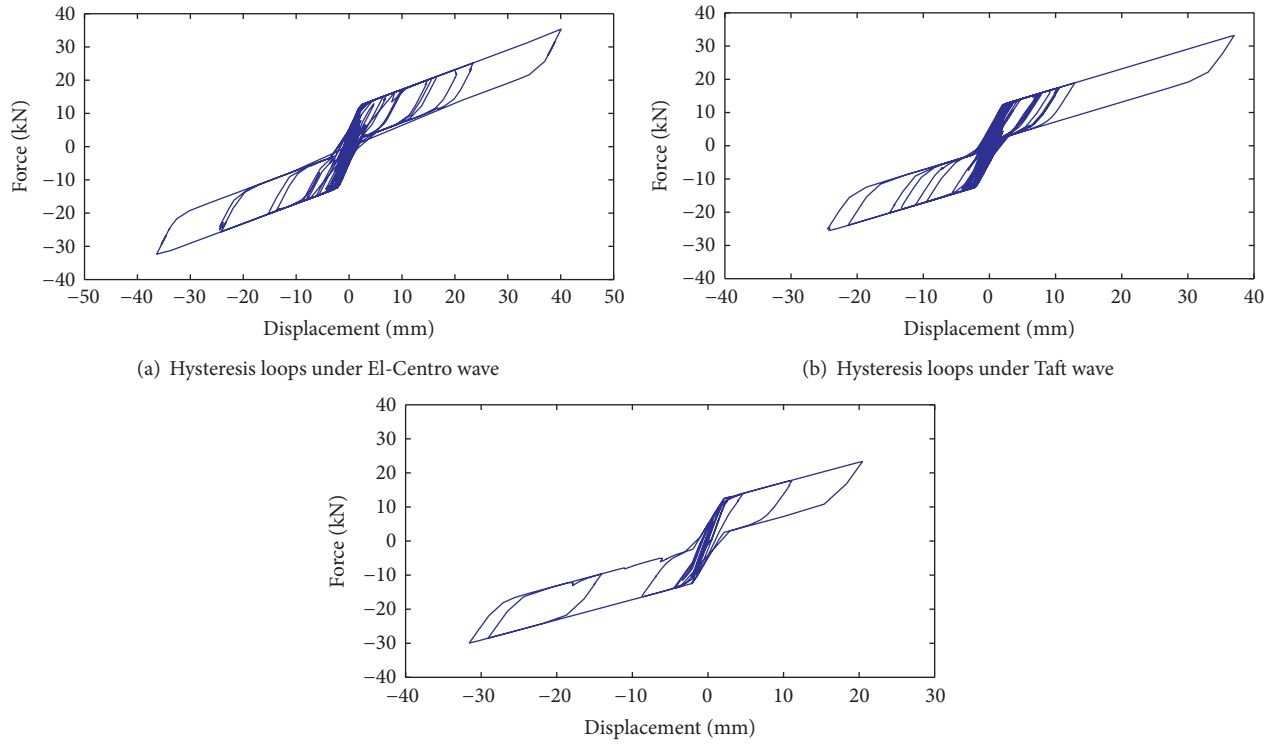

(a) Hysteresis loops under El-Centro wave

(b) Hysteresis loops under Taft wave

(c) Hysteresis loops under Sylmar wave

Figure 13: Force-displacement curves of the SMA spring restrainer under various earthquake wave (PGA = 0.4 g).

Table 4: Control effect of peak axial force under seismic excitations scaled to 0.2 g amplitude (units in kN).

Beam number	El-Centro			Taft			Sylmar		
	Controlled	Uncontrolled	β	Controlled	Uncontrolled	β	Controlled	Uncontrolled	β
1	5.11	6.68	0.235	6.64	7.56	0.122	9.76	11.41	0.145
2	5.03	6.57	0.234	6.65	7.90	0.158	9.65	11.43	0.156
3	3.62	4.22	0.142	3.43	4.58	0.251	2.84	3.23	0.121
4	3.59	4.28	0.161	3.50	4.52	0.226	2.69	3.28	0.180
5	9.92	13.38	0.259	8.36	10.45	0.200	9.34	10.82	0.137

Table 5: Control effect of peak axial force under seismic excitations scaled to 0.3 g amplitude (Units in kN).

Beam number	El-Centro			Taft			Sylmar		
	Controlled	Uncontrolled	β	Controlled	Uncontrolled	β	Controlled	Uncontrolled	β
1	7.56	10.03	0.246	8.07	11.29	0.285	13.82	17.13	0.193
2	7.33	9.83	0.254	8.09	11.78	0.313	13.80	17.18	0.197
3	5.18	6.32	0.180	4.65	6.84	0.320	3.10	4.85	0.361
4	5.19	6.30	0.176	4.67	6.35	0.293	3.11	5.29	0.402
5	13.97	20.07	0.304	12.58	16.65	0.244	13.66	16.25	0.159

Table 6: Control effect of peak axial force under seismic excitations scaled to 0.4 g amplitude (units in kN).

Beam number	El-Centro			Taft			Sylmar		
	Controlled	Uncontrolled	β	Controlled	Uncontrolled	β	Controlled	Uncontrolled	β
1	8.02	13.36	0.400	9.38	15.07	0.378	15.78	22.89	0.311
2	8.39	13.09	0.359	9.65	15.73	0.387	15.64	22.87	0.316
3	6.86	8.46	0.189	5.31	9.13	0.418	4.55	7.30	0.377
4	6.90	8.55	0.193	5.32	8.28	0.358	4.20	7.24	0.420
5	16.56	26.75	0.381	13.46	20.88	0.355	15.34	21.61	0.290

seismic excitation cases. It can be observed that the seismic restrainer exhibits perfect superelastic behavior, which is greatly important for recentering control of the friction isolation system. Moreover, note that the displacement amplitudes of the superelastic restrainer are still kept in the design deformation range during strong earthquakes.

5. Conclusions

This study presents seismic performance analysis of a single-layer spherical lattice shell controlled by flat sliding isolation bearings and SMA spring restrainers. This investigation discusses a simplified analytical approach for modeling the superelastic seismic restrainer that can be used in the seismic analysis of the controlled lattice shell. The controlled and uncontrolled lattice shell structures are analyzed for moderate and strong earthquake ground motions. The numerical results show that the installed isolation and control devices are capable of mitigating peak nodal acceleration response, dynamic internal force of beam element of the lattice shell roof, and base shear response of the structure, while effectively restraining peak displacement response of the friction isolators for all analytical cases. Also, it can be found that the residual displacements of the isolation device are almost zero in all cases considered in this study, demonstrating that the recentering capability and large deformation property of the proposed superelastic seismic restrainer can be effectively used to eliminate the permanent deformation in sliding isolators and protect the lattice shell structure from earthquake damage.

Competing Interests

The authors declare that they have no competing interests.

Acknowledgments

The authors gratefully acknowledge the support from Beijing Natural Science Foundation under Grant no. 8132024 and the Science and Technology Development Project of Beijing Municipal Commission of Education under Grant no. KM201510016004.

References

[1] American Association of State Highway and Transportation Officials, *Guide Specifications for Seismic Isolation Design*, American Association of State Highway and Transportation Officials, Washington, DC, USA, 1999.

[2] T. T. Soong and G. F. Dargush, *Passive Energy Dissipation Systems in Structural Engineering*, John Wiley & Sons, New York, NY, USA, 1997.

[3] E. Graesser and F. Cozzarelli, "Shape memory alloys as new materials for aseismic isolation," *Journal of Engineering Mechanics*, vol. 117, no. 11, pp. 2590–2608, 1991.

[4] M. Dolce, D. Cardone, and R. Marnetto, "Implementation and testing of passive control devices based on shape memory alloys," *Earthquake Engineering and Structural Dynamics*, vol. 29, no. 7, pp. 945–968, 2000.

[5] R. DesRoches, J. McCormick, and M. Delemont, "Cyclic properties of superelastic shape memory alloy wires and bars," *Journal of Structural Engineering*, vol. 130, no. 1, pp. 38–46, 2004.

[6] S. Xue and X. Li, "Control devices incorporated with shape memory alloy," *Earthquake Engineering and Engineering Vibration*, vol. 6, no. 2, pp. 159–169, 2007.

[7] F. Casciati, L. Faravelli, and K. Hamdaoui, "Performance of a base isolator with shape memory alloy bars," *Earthquake Engineering and Engineering Vibration*, vol. 6, no. 4, pp. 401–408, 2007.

[8] Y. Ding, X. Chen, A. Li, and X. Zuo, "A new isolation device using shape memory alloy and its application for long-span structures," *Earthquake Engineering and Engineering Vibration*, vol. 10, no. 2, pp. 239–252, 2011.

[9] O. E. Ozbulut and S. Hurlebaus, "Optimal design of superelastic-friction base isolators for seismic protection of highway bridges against near-field earthquakes," *Earthquake Engineering and Structural Dynamics*, vol. 40, no. 3, pp. 273–291, 2011.

[10] A. Bhuiyan and M. Alam, "Seismic vulnerability assessment of a multi-span continuous highway bridge fitted with shape memory alloy bars and laminated rubber bearing," *Earthquake Spectra*, vol. 28, no. 4, pp. 1379–1404, 2012.

[11] M. Speicher, D. E. Hodgson, R. Desroches, and R. T. Leon, "Shape memory alloy tension/compression device for seismic retrofit of buildings," *Journal of Materials Engineering and Performance*, vol. 18, no. 5-6, pp. 746–753, 2009.

[12] G. Attanasi and F. Auricchio, "Innovative superelastic isolation device," *Journal of Earthquake Engineering*, vol. 15, supplement 1, pp. 72–89, 2011.

[13] R. Mirzaeifar, R. DesRoches, and A. Yavari, "A combined analytical, numerical, and experimental study of shape-memory-alloy helical springs," *International Journal of Solids and Structures*, vol. 48, no. 3-4, pp. 611–624, 2011.

[14] Y.-K. Wen, "Method for random vibration of hysteretic system," *Journal of the Engineering Mechanics Division*, vol. 102, no. 2, pp. 249–263, 1976.

[15] M. Constantinou, A. Mokha, and A. Reinhorn, "Teflon bearings in base isolation II: modeling," *Journal of Structural Engineering*, vol. 116, no. 2, pp. 455–474, 1990.